

e^+e^- PHYSICS BELOW Z^0

K.Abe

National Laboratory for High Energy Physics
Tsukuba, Ibaraki 305 Japan

Abstract

Recent results on e^+e^- physics from PEP, PETRA, and TRISTAN are reviewed. Electroweak couplings in e^+e^- going to $\mu^+\mu^-$, $\tau^+\tau^-$, $c\bar{c}$, $b\bar{b}$, and $q\bar{q}$ are in good agreement with the standard model. Multihadron event shapes are well described by a Monte Carlo model consisting of the parton shower generation and the string fragmentation. This type of model can reproduce even detailed aspects of the hadronization such as the soft gluon emission, the intermittency, and the strange baryon correlations. Different methods of measuring $\Lambda_{\overline{MS}}$ give consistent values with each other. The strong coupling constants measured in the c - and b -quarks are consistent with the flavor-independence of the QCD coupling. The analysis of four-jet events confirms non-Abelian nature of QCD. Difference of the gluon fragmentation from that of the quark is observed.

1. Introduction

Investigations on e^+e^- physics below Z^0 have been actively pursued at PEP, PETRA, and TRISTAN. Their activities cover the electroweak couplings, new particle search, and the QCD effects. After SLC and LEP became operational in 1989, the effort was confined to a detailed study of the electroweak interference effects and the various QCD effects. A wide energy range covered by the three accelerators have been extremely valuable since both the electroweak effects and the QCD effects depend on the center-of-mass energy. TRISTAN, after accumulated about 33 pb^{-1} between 50 and 64 GeV during its energy scan, switched to a high luminosity mode of running at 58 GeV in 1989 and accumulated additional 30 pb^{-1} so far. The PETRA experiments have been finalizing their high statistics studies on several subjects using 86 pb^{-1} data at 35 GeV, even though they stopped running in 1986. Results of detailed studies from 300 pb^{-1} at 29 GeV of PEP machine have also been coming out. TPC/ 2γ group continues to accumulate data at PEP.

In this talk, I will review the results from PEP, PETRA, and TRISTAN with strong emphasis on new results since the 1989 SLAC lepton photon conference.

2. R measurements

All available results of R measurements above 9 GeV are shown in Figure 2.1 in terms of energy-combined values. Data of CESR and DORIS are

taken from Ref.1. Data from PEP and PETRA are taken from Ref. 2 and 3. Published values from these experiments were adjusted to the values which would have been obtained if the same radiative correction program of BJK[4] including Z^0 exchange, but excluding the effects of final state radiation, is used. The TRISTAN data, both published results[5] and preliminary results from their most recent run at 58 GeV were obtained by using the FS radiative correction program[6] that includes full electroweak diagrams up to $O(\alpha^3)$. This calculation requires Z^0 mass, top mass, and Higgs mass as the input. Unfortunately all three groups used different values and, thus, combined data from three groups were obtained by adjusting these results to the values at $m_t = 150\text{ GeV}/c^2$, $m_Z = 91.1\text{ GeV}/c^2$, and $m_H = 100\text{ GeV}/c^2$. The solid line curve in Fig.2.1 is the standard model prediction that was calculated by using $m_Z = 91.1\text{ GeV}/c^2$, $\sin^2\theta_W = 0.23$, and $\Lambda_{\overline{MS}} = 300\text{ MeV}$. Agreement between the measurements and the prediction is excellent.

3. Tests of Electroweak Parameters

3.1 Forward-backward Asymmetry and R in $\mu^+\mu^-$ and $\tau^+\tau^-$

The pure leptonic processes $e^+e^- \rightarrow \mu^+\mu^-$ and $e^+e^- \rightarrow \tau^+\tau^-$ are the cleanest reactions for examining the electroweak couplings. The production cross section and the forward-backward asymmetry are described by

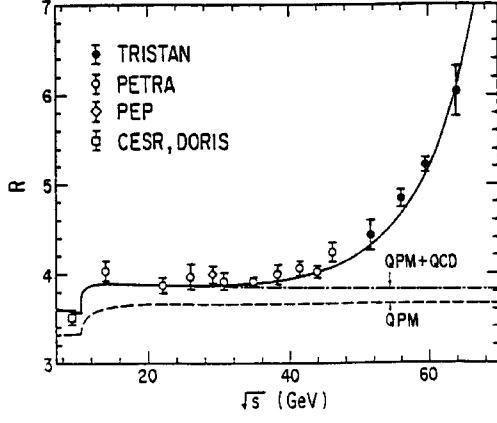


Fig.2.1 The result of R measurements at CESR, DORIS, PEP, PETRA, and TRISTAN. The standard model prediction that is obtained by using $m_Z=91.1\text{GeV}/c^2$, $\sin^2\theta_W=0.23$, and $\Lambda_{\overline{MS}}=300\text{MeV}$ is also shown.

$$R_{ll} = 1 + 8v_e v_l R_e \chi + 16(v_e^2 + a_e^2)(v_l^2 + a_l^2)\chi^2, \quad (3.1)$$

$$A_{ll} = [6a_e a_l R_e \chi + 48v_e v_l a_e a_l \chi^2] / R_{ll} \quad (3.2)$$

where v and a are for the vector and axial vector couplings and

$$\chi = \frac{1}{16\sin^2\theta_W \cos^2\theta_W} \frac{s}{(s - m_Z^2)} \quad (3.3)$$

is the Z^0 contribution. The coupling constants determined at Z^0 , which were measured very precisely at recent LEP experiments, should reproduce R_{ll} and A_{ll} in the region of PEP, PETRA, and TRISTAN completely if the standard model is correct. Figure 3.1 show all available data [7] together with the standard model predictions.

Validity of the standard model can be tested in different ways. Here we fix the Z^0 contribution χ by fixing the values of m_Z , Γ_Z , and $\sin^2\theta_W$ as $91.1\text{GeV}/c^2$, 2.5 GeV , and 0.23 respectively, but assume that the vector- and axial-vector coupling constants for e , μ , and τ are not known. We try a simultaneous fit to A_{ll} and R_{ll} using all available data with 6 parameters, $v_e v_l$, $a_e a_l$, and a cross term $v_e^2 a_l^2 + a_e^2 v_l^2$ ($l=\mu, \tau$). The result of the fit is shown in Figure 3.2, where projections of 68% CL and 95% CL contours to the $a_e a_l$ vs $v_e v_l$ plane at the best fit value for the cross term are plotted.

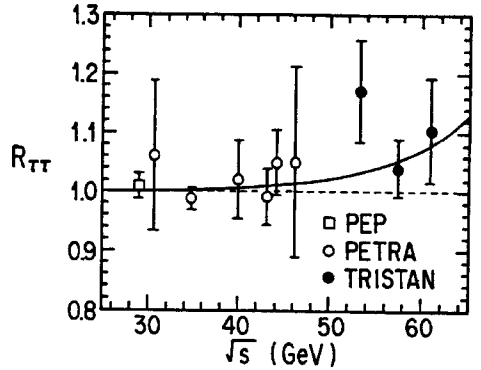
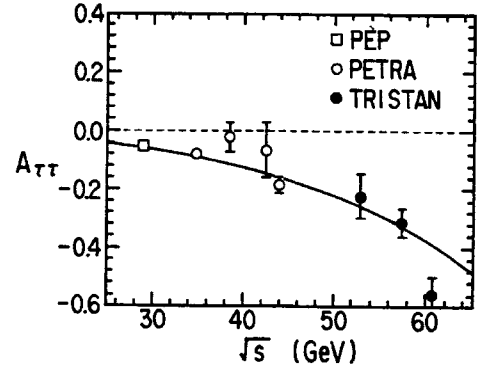
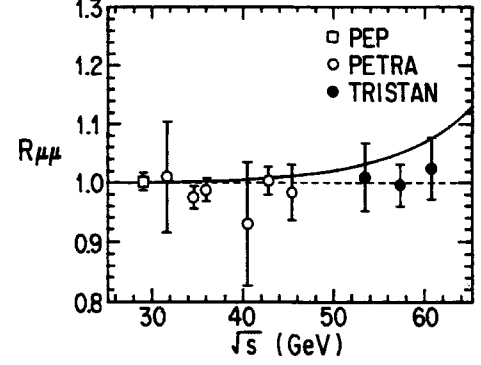
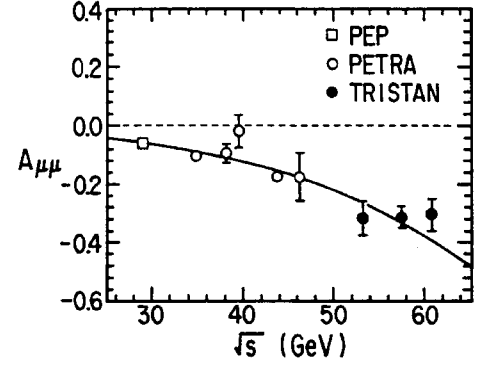


Fig.3.1 The result of forward-backward asymmetry and R_{ll} measurements in $e^+e^- \rightarrow \mu^+\mu^-$ and $e^+e^- \rightarrow \tau^+\tau^-$. The solid line curves are the standard model predictions.

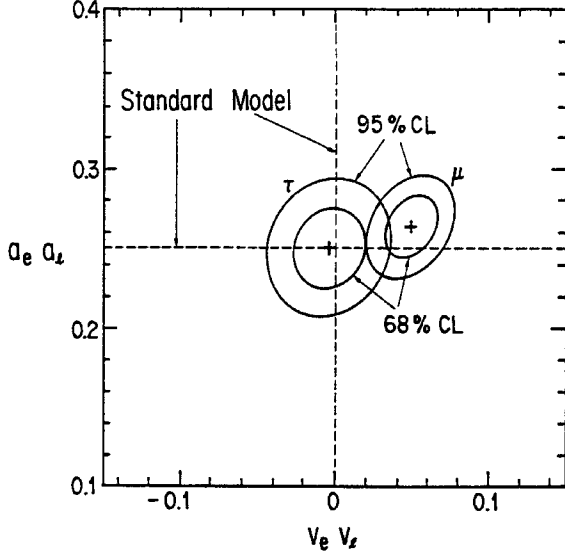


Fig.3.2 Results of the fit in $a_e a_l$ vs $v_e v_l$ plane where $l = \mu, \tau$. The 68% confidence level contours are drawn.

While the result for the tau coupling agrees well with the standard model expectation, that for the muon deviates considerably. If we allow the projection to be drawn from the widest part in the contour as the cross term is varied, the discrepancy becomes less significant. It is estimated that the discrepancy has the statistical significance of 2σ or larger.

As can be seen in Figure 3.3, this is mainly due to a tendency that the measured $R_{\mu\mu}$ in PETRA and TRISTAN are lower than expected. Whether it is just a statistical fluctuation or a real effect remains to be seen. However, if it is a real effect, it must come from some phenomenon other than the electroweak coupling, because the best fitted parameters give $R_{\mu\mu}$ which is two times larger than the precisely measured value at the Z^0 peak. The corresponding $A_{\mu\mu}$ becomes +30% which is also rejected by the recent measurements. The fit was repeated by assuming $e - \mu - \tau$ universality. The result of two parameter fit is shown in Figure 3.4. Even though the value of the axial coupling constant is tightly constrained to a region expected from the standard model, that of the vector coupling constant has a large ambiguity.

Testing the validity of the radiative correction is an important test of the standard model. JADE group used their high statistics data sample of

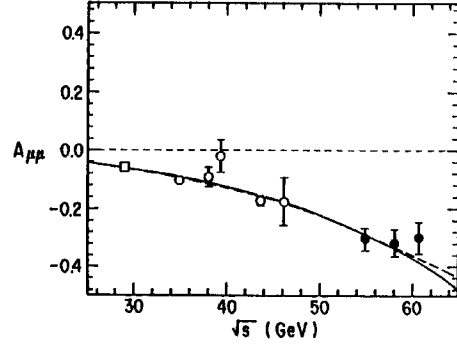
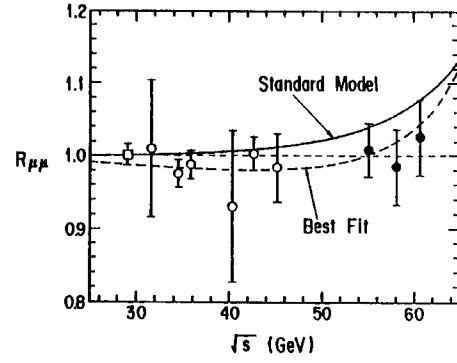


Fig.3.3 $R_{\mu\mu}$ and $A_{\mu\mu}$ together with the standard model prediction (solid lines) and with the best fit (dotted lines.)

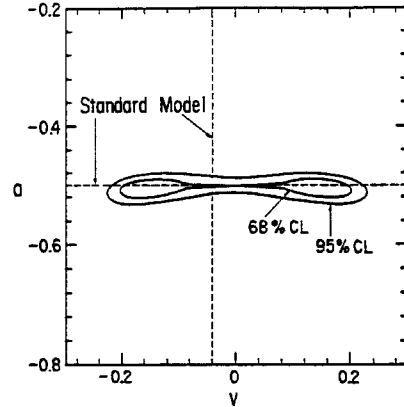


Fig.3.4 Results of the fit assuming $e - \mu - \tau$ universality. Contours of 68%CL and 95%CL are drawn.

$e^+e^- \rightarrow \mu^+\mu^-$ at $\sqrt{s}=35$ GeV to study an effect of acollinearity cut on the $A_{\mu\mu}$. Figure 3.5(a) shows the acollinearity distribution between the outgoing μ^+ and μ^- together with a calculation including the radiative correction. The agreement is good. In Figure 3.5(b), $A_{\mu\mu}$ calculated at three different region of acollinearity are shown. Events with small acollinearity do not contain hard photon radiation and an interference between the tree diagram and the box diagram is positive and this effect tends to reduce the electroweak asymmetry. This tendency is clearly seen in the data and it has good agree-

ment with the Monte Carlo prediction. In the larger acollinearity region in which events contain the hard photon emission, an interference between the initial and final state radiation is negative and tends to increase the $A_{\mu\mu}$. As acollinearity increases further, the definition of θ angle becomes inaccurate and effectively reduces $A_{\mu\mu}$. These effects are clearly seen in the data.

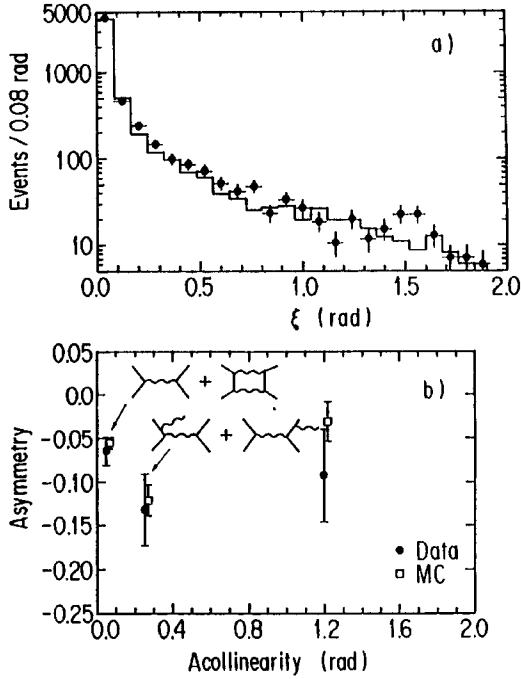


Fig.3.5 Acollinearity distribution in $e^+e^- \rightarrow \mu^+\mu^-$ measured by JADE group(a). $A_{\mu\mu}$ in different region of the acollinearity(b).

3.2 Forward-backward Asymmetry in $c\bar{c}$

Measurements of the forward-backward asymmetry in $e^+e^- \rightarrow c\bar{c}$ requires tagging of the c-quark. This can be achieved either by directly reconstructing $D^{*\pm}$ meson or by observing a soft pion from the decay of $D^{*\pm} \rightarrow D^0\pi_s^\pm$. It can also be extracted from the combined analysis of $c\bar{c}$ and $b\bar{b}$ in the inclusive lepton event sample. Results so far reported[8] are summarized in Table 3.1 and plotted in Figure 3.6 after being combined in the center-of-mass energy. Agreement with the standard model prediction which is drawn in a solid line is good especially for the high statistics data at PEP and PETRA.

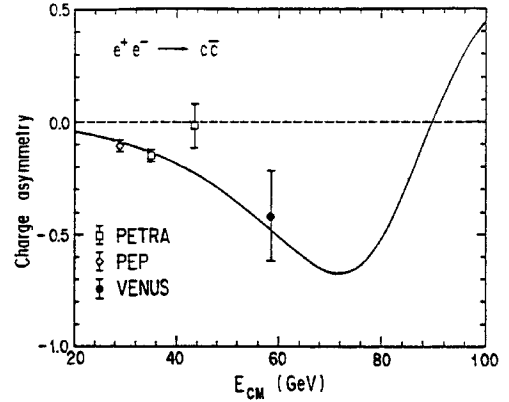


Fig.3.6 The forward-backward asymmetry in $e^+e^- \rightarrow c\bar{c}$. Data are combined in E_{cm} . The standard model prediction is given by the solid line curve.

Table 3.1 Results on the forward-backward asymmetry in $e^+e^- \rightarrow c\bar{c}$. \sqrt{s} is in GeV and A_c is in %.

group	\sqrt{s}	A_c	method
HRS	29	-0.099 ± 0.027	$D^{*\pm}, \pi_s$
TPC	29	-0.140 ± 0.149	μ
TPC	29	-0.210 ± 0.158	e
TPC	29	-0.160 ± 0.160	$D^{*\pm}$
JADE	35	-0.149 ± 0.067	$D^{*\pm}$
JADE	35	-0.123 ± 0.036	e, μ
CELLO	35	-0.146 ± 0.106	$D^{*\pm}, \pi_s$
CELLO	35	-0.129 ± 0.088	e, μ
TASSO	35	$-0.168 \pm 0.047 \pm 0.027$	$D^{*\pm}, \pi_s$
TASSO	43	$+0.077 \pm 0.14$	e, μ
JADE	44	-0.091 ± 0.113	e, μ
VENUS	58.5	-0.42 ± 0.20	$D^{*\pm}$

3.3 Forward-backward Asymmetry in $b\bar{b}$

All available results on the forward-backward asymmetry in $e^+e^- \rightarrow b\bar{b}$ were obtained from analysis using the inclusive lepton events.[9] They are summarized in Table 3.2 and shown in Figure 3.7 after being combined in the center-of-mass energy. Here the deviation from the standard model prediction which is drawn in a solid line is visible, especially for high statistics points at PEP and PETRA. The observed asymmetry by lepton tagging is reduced from the standard model by the $B^0\bar{B}^0$ mixing. The mixing is described by

$$\chi_l = \frac{\Gamma(B^0 \rightarrow \bar{B}^0 \rightarrow l^+)}{\Gamma(B^0 \rightarrow l^- \text{ or } l^+)} = f_d \chi_d + f_s \chi_s, \quad (3.4)$$

here d and s are for B_d and B_s mesons and f_d and f_s are the fractions of B_d and B_s mesons in the neutral B mesons. The observed asymmetry is related to the standard model prediction by

$$A_{obs} = A_{SM}(1 - 2\chi_l). \quad (3.5)$$

The dotted curve in Figure 3.7 is obtained by fitting all available A_b data to the equation (3.5). The result of the fit gives $\chi_l = .131 \pm .054$. Table 3.3 summarizes the measurements of χ_l by various methods.[10]

Fractions f_d and f_s can be estimated by making two reasonable assumptions; i) probabilities for $b\bar{b}$ quark pair picks $u\bar{u}$, $d\bar{d}$, $s\bar{s}$ are 1:1:0.3, ii) semileptonic branching fractions are same for B_d and B_s mesons. These assumptions give $f_d = 0.375$ and $f_s = 0.15$. The region of r_d - r_s plane which is allowed by $\chi_l = .139 \pm .032$ is shown in Figure 3.8(a). Here $r = \Gamma(B^0 \rightarrow l^+)/\Gamma(B^0 \rightarrow l^-)$ and χ are related by $r = 1/(1 - \chi)$. The allowed region from $r_d = .169 \pm .038$, which is obtained by averaging CLEO and ARGUS result, is also shown. From a combined fit of these two constraints, an allowed region in r_d - r_s plane with 1σ and 90%CL are given as shown in Figure 3.8(b). From this analysis, $r_s = 0$ is excluded with 95%CL and a preferred value of r_s is 1.0 as is predicted by the standard model.

3.4 Quark Charge Asymmetry

The quark charge asymmetry, summed over flavours, serves as a good consistency check for electroweak-couplings, quark-universality among up-types and down-types, and the hadronization mechanisms. The observed asymmetry can be interpreted as a sum of contributions from all flavours

$$A_h = f_d A_d - f_u A_u + f_s A_s - f_c A_c + f_b A_b, \quad (3.6)$$

where f_i are proportions with which quark flavours are produced, and A_i are their asymmetries. Negative signs in front of the up-type quark terms are due to the fact that experimentally only charge of the jet, not quark or anti-quark, can be determined and thus θ is defined as the angle of outgoing positively charged jet with respect to the incoming positron. This fact causes a near cancellation of the combined asymmetry, resulting +1% to +10% in the energy region of PEP, PETRA, and TRISTAN.

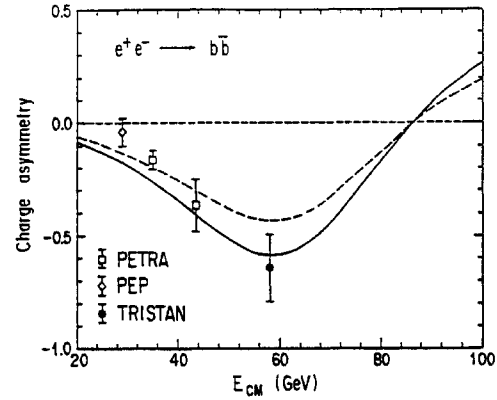


Fig.3.7 The forward-backward asymmetry in $e^+e^- \rightarrow b\bar{b}$. Data are combined in E_{cm} . The standard model prediction is given by the solid line curve. Result of a fit to all available data by allowing the $B^0 - \bar{B}^0$ mixing as a free parameter is shown by dotted line curve.

Table 3.2 Results on the forward-backward asymmetry in $e^+e^- \rightarrow b\bar{b}$.

group	\sqrt{s}	A_b	method
HRS	28	$-.140 \pm .120$	e
MAC	29	$+.034 \pm .078$	μ
TPC	29	$-.150 \pm .206$	μ
TPC	29	$-.360 \pm .352$	e
JADE	35	$-.116 \pm .048$	e, μ
CELLO	35	$-.222 \pm .081$	e, μ
TASSO	35	$-.21 \pm .08$	e, μ, ν, τ, χ
CELLO	43	$-.491 \pm .165$	e, μ
AMY	57.2	$-.82 \pm .25 \pm .14$	μ
TOPAZ	58.9	$-.64 \pm .32 \pm .10$	μ
VENUS			e, μ

Table 3.3 Measurements of χ_l .

experiment	method	χ_l
UA1	dilepton	$.121 \pm .047$
MAC	dilepton	$.21 \pm .29 \pm .15$
MARK II	dilepton	$.17 \pm .15 \pm .08$
	fit to A_b	$.131 \pm .054$
	average	$.139 \pm .032$

Figure 3.9 shows all available results[11] as a function of \sqrt{s} . These results are the corrected val-

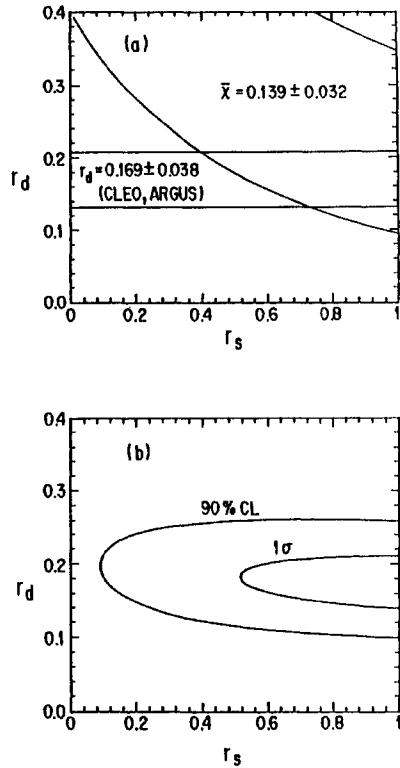


Fig.3.8(a) Allowed region in $r_d - r_s$ plane determined by averaged χ_I and by the $B_d \bar{B}_d$ mixing which was measured by both CLEO and ARGUS. (b) 1σ and 90%CL contours from simultaneous fit of average χ_I and $B_d \bar{B}_d$ mixing.

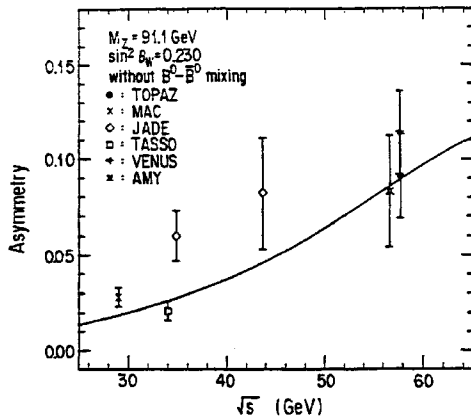


Fig.3.9 Measurements of quark charge asymmetry vs \sqrt{s} . The solid line curve represents the standard model prediction that is calculated without including an effect of $B^0 \bar{B}^0$ mixing.

ues for the probabilities of charge identification and misidentification and for selection efficiencies for each flavour. Thus they can be compared directly with the standard model prediction. Overall agreement between the observation and the prediction is a good evidence that the electroweak properties of each of five flavours and an assumed hadronization scheme are correct.

3.5 Quark Bremsstrahlung

TASSO and JADE[12] obtained clear evidence for the presence of bremsstrahlung photons emitted by the primary quarks. A high statistics study by JADE at $\sqrt{s}=35\text{GeV}$ attributes 128 ± 41 events out of 723 hadronic events with an isolated photon in the range of $0.2 \leq x \leq 0.8$ to the quark bremsstrahlung. Here x is the photon energy divided by the beam energy. Small x and large x region were removed from the analysis in order to reduce contaminations from π^0 and η and from the initial state radiation. The x distribution is shown in Figure 3.10 together with the Monte Carlo simulation with and without the quark bremsstrahlung. It can be seen that the observed distribution prefers the prediction including the quark bremsstrahlung.

The quark charge asymmetry for hadronic events containing hard photon emission is expected to become negative due to an interference between the contribution from the initial state radiation (charge conjugation of the hadron state, $C=-1$) and the contribution from the quark bremsstrahlung ($C=+1$). Figure 3.11 shows $\cos\theta_{jet}$ distribution obtained from the JADE data together with the Monte Carlo expectation. An asymmetry of $A=-0.141 \pm 0.041$ is observed, which agrees well with the expected value of $A=-0.122 \pm 0.014$.

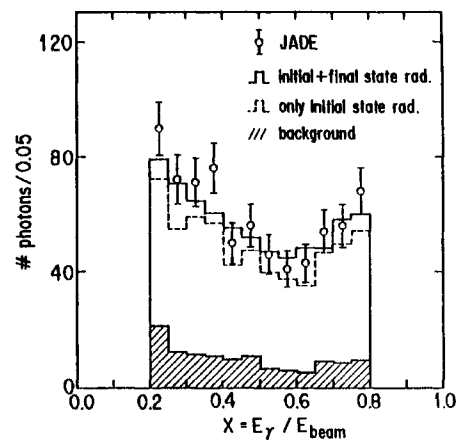


Fig.3.10 The spectrum of isolated photon in multi-hadron events measured by JADE group. Data are plotted together with the predictions including initial state radiation only and both initial and final state radiation.

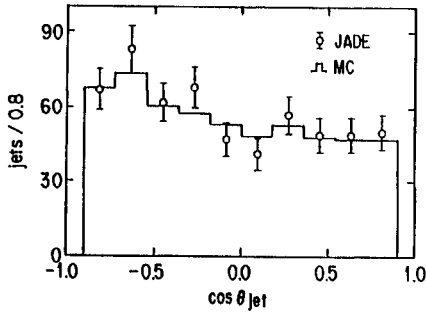


Fig.3.11 $\cos\theta_{jet}$ distribution of multi-hadron events containing an isolated photon. θ_{jet} is defined as an angle of a positively charged jet with respect to the positron direction.

4. Multihadron Event Properties

4.1 Monte Carlo Models

It has been well established that in the PEP and PETRA energy region, the Lund parton-shower model(PS), which is based on the leading-logarithm-approximation(LLA) of the QCD cascade approach and the string fragmentation, reproduces wide variety of event shape distributions. This tendency remains to hold even at the TRISTAN energies. In fact it is not necessary to re-tune the model parameters determined at PETRA in order to reproduce most of the event shape distributions observed at TRISTAN.[13] Recently, significant amount of effort was made to explore the hadron formation mechanism even further, both at the parton level and at the hadronization level. It is remarkable to see that the Lund PS model can reproduce some detailed aspects of the data as are described in this chapter.

4.2 Soft Collinear Gluon-emission

TPC/2 γ group observed a significant dip in the rapidity distributions of charged pions at $y \approx 0$ for events with low sphericity.[14] The rapidity distributions for different regions of sphericity are shown in Figure 4.1. For this measurement, it is important to positively identify pions because misidentified kaons and protons give large y and therefore generate artificial dips at $y \approx 0$. Pure $q\bar{q}$ tends to give a flat rapidity distributions near $y = 0$ and in order to generate a dip, it is necessary to have 3 to 4 soft gluons which are correctly angular-ordered. Their study indicated that only Lund parton-shower model in which partons are evolved down to $Q \approx 1$ GeV can reproduce

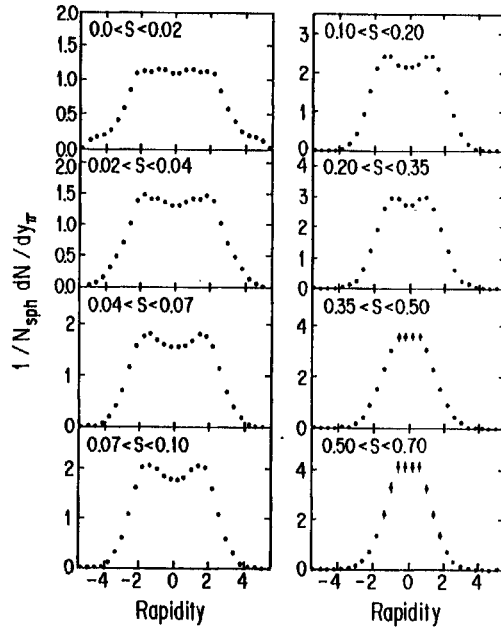


Fig.4.1 Rapidity distributions of charged pions in planar events for different sphericity bins measured by TPC/2 γ group.

the observed dips correctly.

4.3 Intermittency

After unusually large density fluctuations of the rapidity were observed in cosmic ray events, in hadron-hadron, and nucleus-nucleus collisions[15], Bialas and Pechanski[16] suggested that by studying the factorial moments at different bin-sizes(resolution scale) one can distinguish an effect of dynamical origin from pure statistical fluctuation. Since this effect was likely related to the hadronization mechanism, it was immediately realized an importance of studying it in multihadron events in e^+e^- annihilation where most of the hadronization properties are well described by the existing Monte Carlo calculation. The first direct evidence of intermittency in e^+e^- interaction was reported by TASSO group[17]. Figure 4.2 shows the factorial moments of rank 2-4 calculated from the rapidity distribution with respect to the sphericity axis, y , as a function of the number of bins. The factorial moment of i -th rank is defined by

$$F_i = \left\langle \frac{1}{M} \sum_{m=1}^M \frac{n_m(n_m-1)\dots n_{m-i+1}}{N(N-1)\dots(N-i+1)} M^i \right\rangle, \quad (4.1)$$

where M is the number of bins, N is the number of tracks in the event, n_m is the entry in m -th bin, and $\langle \rangle$ means averaging over all events. Only charged particles in the region $-2 \leq y \leq 2$ were used in the calculation. The detector resolution for determining the rapidity σ_y is 0.04.

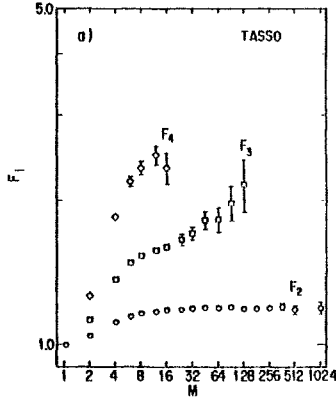


Fig.4.2 Factorial moments of rank 2, 3, and 4 vs number of bins in rapidity measured by TASSO group. Only charged tracks are used and the rapidity is calculated with respect to sphericity axis. Rapidity range used in this analysis is $-2 \leq y \leq 2$.

These factorial moments should be $F_i \approx 1$ if the fluctuation is purely statistical and $F_i \geq 1$ if there are additional fluctuations of dynamical origin. In the random cascade hadronization, these moments should have a power law behaviour,

$$F_i = AM^{\alpha_i} \quad (4.2)$$

where slopes of different ranks should be related by

$$\alpha_{i+1} - \alpha_i = i\alpha_2. \quad (4.3)$$

As M becomes larger, thus bin size becomes smaller, than the experimental resolution, F_i starts to become flat and eventually becomes constant.

TASSO's observation that F_i is significantly larger than 1 and $F_4 \geq F_3 \geq F_2$ is consistent with the random cascade hadronization. They also calculated the factorial moments in two-dimensional distribution (y, ϕ) , ϕ being the azimuthal angle of the track, and found that they show a same tendency as the one-dimensional case except the effect is much larger. Their observation indicated that, even though the factorial moments calculated from all available hadronization models give some resemblance to the data, none reproduces their data well.

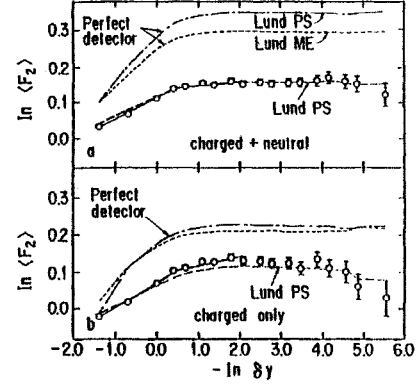


Fig.4.3 Factorial moments of rank 2 measured by CELLO group both for charged tracks only and for charged and neutral tracks. Predictions from parton-shower plus string fragmentation is shown by dashed line. Also shown in the figure are predictions in the case of perfect acceptance and perfect detector resolution for Lund PS and Lund ME. δy is the rapidity interval spanned by one bin.

CELLO has reported results from a similar analysis[18] which is shown in Figure 4.3. A main difference is that CELLO analysis include both charged and neutral tracks. Behaviour of the factorial moments from CELLO's y distribution is consistent with the random cascade hadronization model. Also they are well reproduced by the LUND7.2(parton shower plus string fragmentation).

In order to explore the origin of intermittency further, they studied behaviour of the factorial moments for the three-dimensional($dp_x/\sqrt{E}, dp_y/\sqrt{E}, dp_z/\sqrt{E}$) charge multiplicity distribution[19]. Figure 4.4 shows F_2 - F_5 as function of $\delta LIPS = \Delta LIPS/M^3$, where $\Delta LIPS$ is the original total phase space volume and M^3 is the number of cubes in the phase space. The predictions of the LUND7.2, prior to and after detector simulation are also shown. The agreement is nearly perfect.

They calculated the fractal dimension D_i^F from the slopes α_i by using a relation

$$D_i^F = D_0 \left(1 - \frac{\alpha_i}{i-1} \right), \quad (4.4)$$

here D_0 is the phase space dimension and is 3 in this case. It is shown in Figure 4.5. The D_i^F can be interpreted as a number in which degree of correlation is subtracted from the phase space dimension. It is near zero when the cube size is large and all tracks belong to one cube(perfect correlation). As the cube size becomes smaller, D_i^F increases to nearly 3: reflection of tracks being populated according a phase space distribution over many cubes. If only geometrical property of fragmentation exist, D_i^F should stay

near 3. The observed D_2^F begins to decrease and comes down to near 2, indicating an existence of a short-range correlation. The LUND7.2 reproduces this effect as can be seen in the figure. The Dalitz decay of π^0 was found to be responsible for this effect.

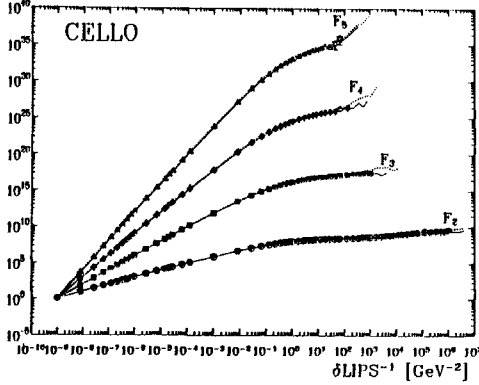


Fig.4.4 Factorial moments obtained from CELLO data using three dimensional variables, p_x/\sqrt{E} , p_y/\sqrt{E} , p_z/\sqrt{E} . Solid line and dotted line curves are for predictions from LUND 7.2 PS after and prior to the detector simulation respectively.

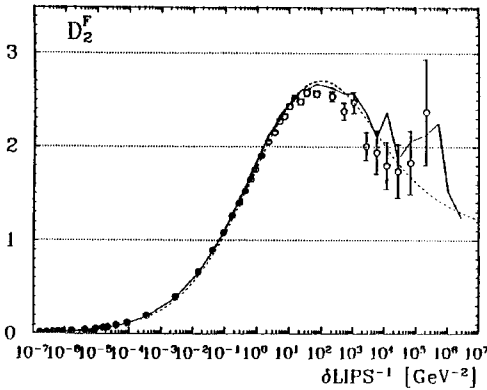


Fig.4.5 Fractal dimension inferred from F_2 .

4.5 Heavy Baryon Productions

Heavy baryons such as strange and charm baryons are likely to have originated from the primary quarks in the e^+e^- annihilation. Therefore they provide a straightforward test of the fragmentation models. Their flavour correlations provide the detailed colour confinement mechanism in the baryon formation process. TPC/2 γ group made a new measurement of the heavy baryon production rates using $70pb^{-1}$ data collected in 1984-1986 at 29 GeV.[20]

Their new measurement and the previous world averages[21] at $\sqrt{s} \sim 29$ GeV are summarized in Table 4.1. Also included in this Table are the predictions from three different models. The Webber model is based on the cluster fragmentation, whereas the Lund PS and the UCLA model are based on the string fragmentation. The UCLA model[22] introduces two additional concepts besides following the string fragmentation; hadronic phase space and a linear confining quark potential. This model does not contain many of quark-level parameters such as s/u or $vector/all$, which are needed in other models.

The two models based on the string fragmentation have better agreement compared with the cluster model in general. Only significant discrepancy between the observation and the prediction is in the Λ_c production. The new TPC/2 γ result is based on reconstructing the $\Lambda_c \rightarrow pK\pi$, whereas the previous result comes from $\Lambda_c \rightarrow \Lambda e^\pm X$ measurement by MARKII. The result at $\sqrt{s} \sim 10$ GeV from ARGUS using $\Lambda_c \rightarrow pK\pi$ gives 0.19 ± 0.08 . [21] Because of different \sqrt{s} , it may not be valid to compare the ARGUS result with the other two. Nevertheless these

Table 4.1 Results on heavy baryon production rate at $\sqrt{s} \sim 29$ GeV as expressed in average number of baryons per one hadronic event.

	Λ^0	Ξ^-	Ω^-	Ξ^{0*}	Λ_c
TPC/2 γ	$.211 \pm .017$	$.020 \pm .005$	$.0037 \pm .0023$	$.0097 \pm .0058$	$.22 \pm .11$
previous ave.	$.208 \pm .014$	$.017 \pm .004$	$.014 \pm .006$	$\leq .006$	$.28 \pm .25$
Webber 4.1	.236	.036	.0053	.022	.043
Lund PS	.217	.018	.0008	.004	.055
UCLA	.180	.012	.0008	.004	.024

three results are compatible with each other and significantly larger than expected. Further study is needed to resolve the discrepancy.

Table 4.2 summarizes the strange baryon correlation data.[21] They are given in terms of the ratio defined as in the Table in order to reduce the possible dependence on the center-of-mass energy. They are a measure of how often baryon strangeness is compensated in an antibaryon. Models of the baryon pair formation use a parameter(popcorn) describing the average number of intermediate mesons between the baryon and antibaryon. They are indicated in the Table. The agreement between the measurements and the prediction is satisfactory at the moment and further study with higher statistics is important for understanding the baryon formation mechanism.

Table 4.2 Results on strange baryon correlations.

	$\frac{2N(\Lambda\bar{\Lambda})}{N(\Lambda)+N(\bar{\Lambda})}$	$\frac{N(\Xi\bar{\Lambda})}{N(\Xi)+N(\bar{\Xi})}$
TPC/2 γ	.50 \pm .12	.45 \pm .00
previous ave	.49 \pm .11 (at \sim 29 GeV)	
	.306 \pm .049 (at \sim 10 GeV)	.65 \pm .19 (at \sim 10 GeV)
Webber 4.1		.56
Lund PS	.49 - .31	.69 - .48
0-1 popcorn		
UCLA	.39	.58
1.8 popcorn		

5. Tests of basic QCD

5.1 $\Lambda_{\overline{MS}}$ measurements

Three different methods of extracting the QCD cutoff parameter, $\Lambda_{\overline{MS}}$, were applied on the data below Z^0 . First method uses all available R values in the energy range covered by CESR, DORIS, PEP, PETRA, and TRISTAN. Contributions to the R from quark partons, electroweak effects, and QCD effects are described by

$$R = 3 \sum_q (Q_q^2 + electroweak) \left[1 + c_1 \left(\frac{\alpha_s}{\pi} \right) + c_2 \left(\frac{\alpha_s}{\pi} \right)^2 + c_3 \left(\frac{\alpha_s}{\pi} \right)^3 + \dots \right] \quad (5.1)$$

where the strong interaction coupling constant, α_s , is related to the fundamental QCD cut-off parameter, $\Lambda_{\overline{MS}}$, through a relation

$$\alpha_s(Q^2) = \frac{12\pi}{(32 - 2N_f) \ln \frac{Q^2}{\Lambda_{\overline{MS}}^2}} \times \left[1 - \frac{6(153 - 19N_f) \ln(\ln \frac{Q^2}{\Lambda_{\overline{MS}}^2})}{(32 - 2N_f)^2 \ln \frac{Q^2}{\Lambda_{\overline{MS}}^2}} \right]. \quad (5.2)$$

While the electroweak effect has a strong \sqrt{s} dependence and becomes as large as 25% at TRISTAN energies, the QCD corrections are in the order of 5%, 0.4%, 1% for 1st, 2nd, and 3rd order terms respectively and has very slow \sqrt{s} dependence. This method has an advantage of not depending on the Monte Carlo hadronization model, even though it lacks a good sensitivity due to the small energy dependence of the QCD terms. Here $N_f=5$ ($N_f=4$ below $\sqrt{s}=11$ GeV) and $Q^2 = s$ were used.

In an analysis which fixes the electroweak part of the R expression with $m_Z=91.1$ GeV/ c^2 , $\sin^2\theta_W=0.23$, $m_t=150$ GeV/ c^2 , and $m_H=100$ GeV/ c^2 , the best fit is obtained with $\Lambda_{\overline{MS}} = 380_{-190}^{+240}$ MeV.[23] An alternative approach, which is tried by TOPAZ, fixes only $m_Z=91.1$ GeV/ c^2 and $m_H=100$ GeV/ c^2 and the rest of the electroweak effect is parameterized as a function of m_t . The result is $\Lambda_{\overline{MS}} = 354_{-194}^{+289}$ MeV.[24]

The second method extracts $\Lambda_{\overline{MS}}$ from the asymmetry in the energy-energy correlation. This method has a good sensitivity but a result tends to depend on which hadronization model is used. TOPAZ used the matrix element method by Gottschalk and Shatz and the Lund string fragmentation and obtained $\Lambda_{\overline{MS}} = 209_{-78}^{+104}$ MeV.[25]

The third method is based on a multi-jet analysis. Since a main source of three-jets events is the q $\bar{q}g$ production, the three-jet fraction is sensitive to the value of $\Lambda_{\overline{MS}}$. VENUS performed an analysis using the NLL model.[26] Experimentally determined three-jet fractions vs y_{cut} are compared with the Monte Carlo simulation for different $\Lambda_{\overline{MS}}$. The result is $\Lambda_{\overline{MS}} = 254_{-47}^{+55} \pm 56$ MeV at $\sqrt{s}=58.5$ GeV. Here the first and second error are statistical and systematic respectively. Data and the fits for the multi-jet fractions at $\Lambda_{\overline{MS}}=254$ MeV is shown in Figure 5.1.

5.3 Gluon self-coupling

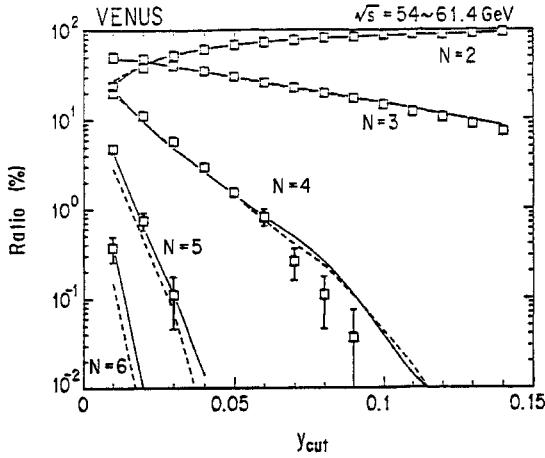


Fig.5.1 The multi-jet fractions vs y_{cut} . Solid lines and dashed lines are the NLL predictions at $\Lambda_{\overline{MS}}=254\text{MeV}$ with and without hadronization.

5.2 Flavour Independence of α_s

The QCD predicts the strong coupling constant α_s to be independent of the flavour. This hypothesis can be tested by comparing the α_s determined from the $q\bar{q}g$ coupling for $c\bar{c}$ or $b\bar{b}$ events, for which several separation techniques are available, to the flavour averaged α_s . TASSO group measured the ratio $\alpha_s(c)/\alpha_s(all)$ and $\alpha_s(b)/\alpha_s(all)$. [27] They tagged $c\bar{c}$ events by identifying $D^{*\pm}$ from a cut on $\Delta M = M(D^0\pi^\pm) - M(D^0)$ and reconstruction of $D^0 \rightarrow K^-\pi^+$ and $D^0 \rightarrow K^-\pi^+\pi^-\pi^+$. Their $b\bar{b}$ events enrichment method utilizes a fact that $b\bar{b}$ events should have a secondary vertex associated with B meson decay in addition to the primary event vertex. Their present resolution does not allow event-by-event tagging, instead they can only obtain $b\bar{b}$ enriched event sample.

The result from these analysis gives

$$\frac{\alpha_s(c)}{\alpha_s(all)} = 0.91 \pm 0.38 \pm 0.15 \quad (5.3)$$

$$\frac{\alpha_s(b)}{\alpha_s(all)} = 1.17 \pm 0.50 \pm 0.28 \quad (5.4)$$

where the first and second errors are statistical and systematic errors respectively. These results are consistent with the strong coupling constant being flavour independent.

According to QCD, the four-jet production cross section should be dominated by a process in which the hard gluon emitted by a quark couples to gg pair. (See Figure 5.2) This is because the gluons themselves carry color charge due to non-Abelian nature of QCD, and thus couple to themselves. It is, however, possible to construct an Abelian model of QCD in which the color factor of the quarks is retained but the color of the gluons is turned off. In this model, the diagram of gluon self-coupling is not allowed and only the coupling of the hard gluon to $q\bar{q}$ pair is allowed. In both non-Abelian and Abelian versions, the double Bremsstrahlung contributions (Figure 5.2(c)) are allowed.

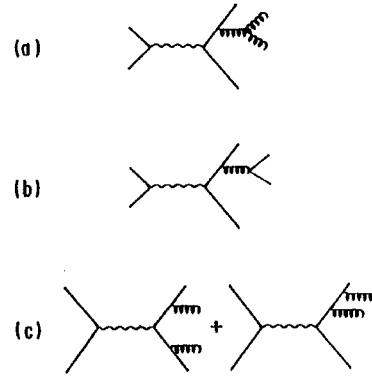


Fig.5.2 Feynman diagrams contributing to four-jet event production.

Bremsstrahlung gluons are polarized along the direction perpendicular to the $q\bar{q}$ plane. When these gluons couple to a $q\bar{q}$ pair, as in Figure 5.2(b), the plane spanned by $q\bar{q}$ pair tends to be perpendicular to the direction of this polarization. On the other hand, when the coupling is to a gg pair as in Figure 5.2(a), the plane spanned by gg pair tends to line up with the direction of the polarization. Experimental analysis is done by ordering the observed four jets according to their visible energies. The two highest energy jets, jet 1 and jet 2, are likely to originate from the primary $q\bar{q}$ pair. The least energetic two, jet 3 and jet 4, are from the gluon conversion and from double Bremsstrahlung processes. The angular correlation can then be observed from the Bengtsson-Zerwas angle, χ , which is defined as an angle between the planes spanned by jet 1 and jet 2, and jet 3 and jet 4, or from the Nachtmann-Reiter angle, θ_{NR}^* , which is defined as an angle between $\mathbf{P}_1 - \mathbf{P}_2$ and $\mathbf{P}_3 - \mathbf{P}_4$.

AMY and VENUS performed this analysis[28]. The χ and θ_{NR} distributions for each separate process determined by VENUS group are shown in Figure 5.3. The partial cross sections for each process are listed in Table 5.1 for QCD and Abelian model. Figures 5.3(c) and (d) compare the VENUS data with the predictions of QCD and Abelian model. Clearly the QCD is preferred.

Table 5.1 The partial cross sections for QCD and Abelian models.

processes	QCD	Abelian Model
$q\bar{q}GG$	28.4%	65.5%
$q\bar{q}Q\bar{Q}$	5.4	34.
$q\bar{q}(G)GG$	66.2	0

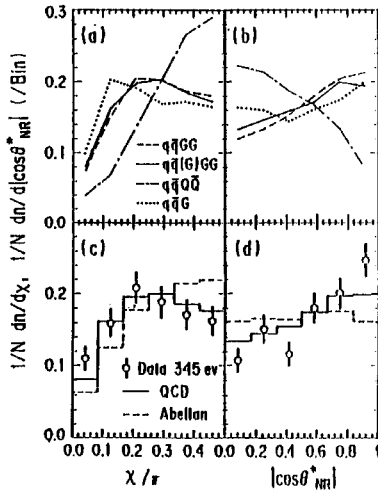


Fig.5.3The χ and $\cos\theta_{NR}$ distributions: (a) and (b) are for each process separately with equal normalization; (c) and (d) are comparisons between data and the predictions of QCD model and Abelian model.

5.4 Different Fragmentation of quarks and gluons

In the infinite energy limit, QCD predicts the multiplicity of gluon fragmentation is 9/4 times larger than that of the quark. Various corrections tend to dilute this effect and reduce this factor to ~ 1.3 in TRISTAN energies. This effect should result as a softer particle spectrum and a wider energy flow in the gluon fragmentation.

TASSO group studied this effect by comparing energy-symmetric three-jet events at $\sqrt{s}=35$ GeV and two-jet events at $\sqrt{s}=22$ GeV.[29] While one jet in the three-jet sample is likely to be a gluon jet, both jets in the two-jet sample are likely to be quark jets. Thus, from these two data, they can extract behavior of the gluon jets. In both samples, the energy which one jet carries is about 11 GeV. Thus this method tends to remove any energy dependent difference between quarks and gluons. Figure 5.4 shows a momentum spectrum of charged tracks within a jet observed by TASSO group. Spectrum from the two-jet, three-jet samples, and the gluon jet sample are shown separately. No difference between quarks and gluons are observed.

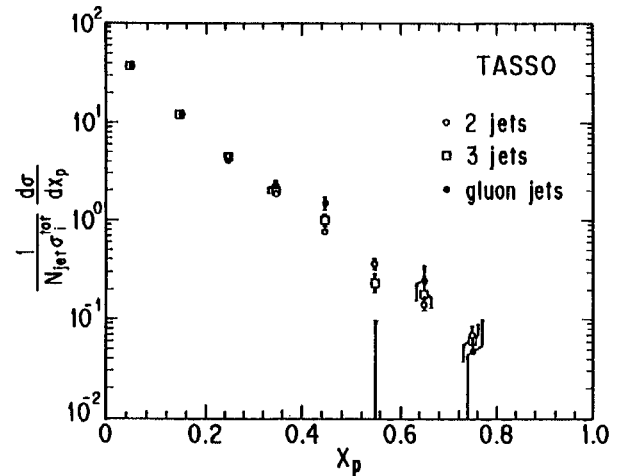


Fig.5.4Momentum spectrum of charged tracks within the jet observed by TASSO

AMY used all 336 three jet events which were selected from 3230 multi-hadron events between 50 and 60.8 GeV.[30] The two highest energy jets(jet-1 and jet-2) in each events are likely to come from the quark fragmentation and the least energetic one(jet-3) from that of the gluons. Thus jets-1 and 2 form a quark-enriched sample and jet-3 forms a gluon enriched sample. They obtained another quark enriched sample from clean two jet events. In this analysis, the energy of gluon jets is lower than that of quarks. In order to avoid any energy dependence of the fragmentation process, they picked variables which are less dependent on the jet energy. Also consideration was given to reduce contribution from soft particles on the studying variables in order to avoid the string effect.

They used the core-energy fraction, ξ , the rapidity of the leading particle, η , and the integrated

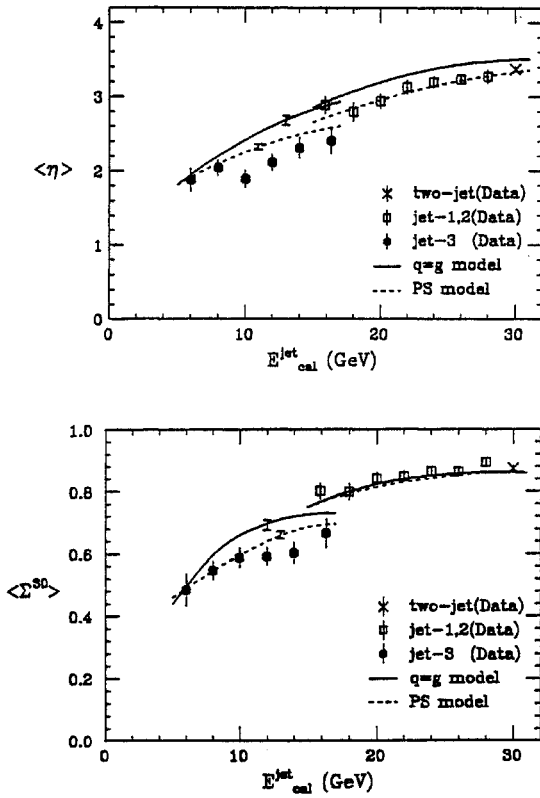


Fig.5.5 Average η and average Σ_{30} distributions versus E_{cal}^{jet} for two jet, jet-1,2, and jet-3 samples.

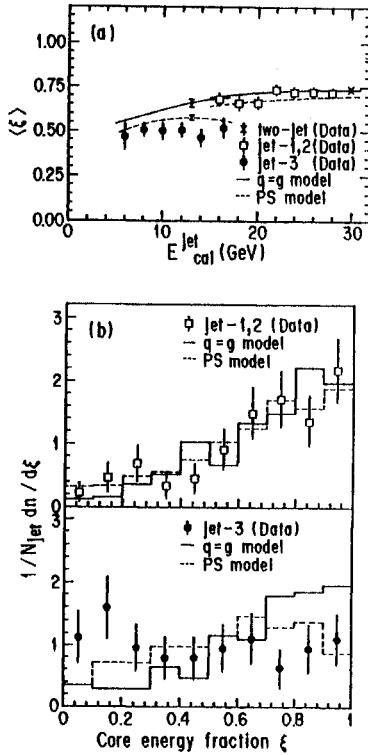


Fig.5.6 Average ξ vs E_{cal}^{jet} (a) and ξ distribution

energy-energy correlation, Σ_{30} , as defined

$$\xi = \frac{\sum_i e_i(\theta_i \leq \theta)}{E_{vis}^{jet}} \quad (5.5)$$

where

$$\theta = \frac{60^\circ}{\sqrt{E_{vis}^{jet}}}, \quad (5.6)$$

$$\Sigma_{30} = \int_0^{30^\circ} \sum_{i,j} \frac{e_i}{E_{vis}^{jet}} \frac{e_j}{E_{vis}^{jet}} \delta(\theta_{ij} - \theta) d\theta. \quad (5.7)$$

Figure 5.5 show average η and average Σ_{30} distributions, both versus E_{cal}^{jet} . Results of three samples, two jet, jet-1,2, jet-3, are plotted. The expectations from two different Monte Carlo calculations are also shown. The $q=g$ model is the Lund 6.2 Matrix Element model with the independent fragmentation scheme of Hoyer *et al.*, and the PS model is the Lund 6.3 Parton Shower model with the string fragmentation. In the $q=g$ model, quarks and gluons are treated in a same way for their hadronization. Thus only difference between quarks and gluons in this model come from the detector effect.

The data shows some difference between the jet-1,2 and the jet-3 in the region of their overlapped E_{cal}^{jet} , while the two-jet is in good agreement with the jet-1,2. The $q=g$ model shows very little difference for all samples as expected and agrees well with the jet-1,2 and the two-jet samples. The differences between the jet-1,2 and the jet-3 are reasonably well reproduced by the PS model, even though the observed differences tend to be greater than the prediction. The difference is most clearly observed in the core energy fraction variable. Figure 5.6(a) shows the average ξ vs E_{cal}^{jet} and figure 5.6(b) shows the distribution of ξ .

6. Conclusion

The electroweak couplings in the processes of e^+e^- going to $\mu^+\mu^-$, $\tau^+\tau^-$, $c\bar{c}$, $b\bar{b}$, and $q\bar{q}$ are in good agreement with the standard model. One possible deviation which has the statistical significance of about 2σ is the larger observed $R_{\mu\mu}$. The hadronization Monte Carlo model based on the parton-shower cascade and the string fragmentation reproduces detailed aspects on the experimental data such as the soft gluon emission, the intermittency, and the strange baryon correlations. Experimental results on

the extraction of $\Lambda_{\overline{MS}}$, the flavour dependence of α_s , the gluon self-coupling, the fragmentation of quarks and gluons, are all consistent with the QCD.

Data taking of e^+e^- annihilation below Z^0 will continue at TRISTAN and PEP for detailed study of the electroweak interference effects and for the hadron formation mechanisms.

References

- [1] R. Giles *et al.*(CLEO), Phys. Rev. **D29**, 1285(1984); P. Boch *et al.*(DESY-Hamburg-MPI-Munich), Z. Phys.**C6**, 125(1980); B. Niczyporuk *et al.*(LENA), Z. Phys. **C15**, 299(1982); C. Berger *et al.*(PLUTO), Phys. Lett. **81B**, 410(1979).
- [2] H. J. Behrend *et al.*(CELLO), Phys. Lett.**183B**, 400(1987).
- [3] W. Bartel *et al.*(JADE), Phys. Lett.**129B**, 145(1983); B. Adeva *et al.*(Mark-J), Phys. Rev. Lett. **50**, 799(1983); R. Brandelik *et al.*(TASSO), Phys. Lett. **113B**, 499(1982); E. Fernandez *et al.*(MAC), Phys. Rev. **D31**, 1537(1983); D. Bender *et al.*(HRS), Phys. Rev. **D31**, 1(1983); L. Criegee and G. Knies, Phys. Rep. **83**, 153(1982).
- [4] F. A. Berends and R. Kleiss, Nucl. Phys. **B178**, 141(1981); F. A. Berends, R. Kleiss and S. Jadach, Nucl. Phys. **B202**, 63(1982).
- [5] T. Kumita *et al.*(AMY), Phys.Rev. **D42**, 1339(1990); I. Adachi *et al.*(TOPAZ), Phys. Lett. **B234**, 525 (1990); K. Abe *et al.*(VENUS), Phys.Lett. **B234**, 382 (1990).
- [6] J. Fujimoto and Y. Shimizu, Mod. Phys. Lett. **A3**, 581(1988).
- [7] A. Bacala *et al.*(AMY), Phys. Lett. **B218**, 112 (1989); I. Adachi *et al.*(TOPAZ), Phys. Lett. **B208**, 319 (1988); K. Abe *et al.*(VENUS), KEK Preprint 89-192, to be published in Z. Phys. C.
- [8] P. Baringer *et al.*(HRS), Phys. Lett. **B206**, 551(1988); H. Aihara *et al.*(TPC), Phys. Rev. **D34**, 1945(1986); H. Aihara *et al.*(TPC), Z. Phys. **C27**, 39(1985); H. Aihara *et al.*(TPC), Phys. Rev. **D31**, 2719(1985); F. Ould-Saada *et al.*(JADE),Z.Phys.**C44**,567(1989); H. J. Behrend *et al.*(CELLO), DESY 89-125; H. J. Behrend *et al.*(CELLO), contribution paper to this conf.; W. Braunschweig *et al.*(TASSO), Z.Phys. **C44**, 365(1989); VENUS, private communication.
- [9] H. R. Band *et al.*(MAC), Phys. Lett.**B218**, 369(1989); C. R. Ng *et al.*(HRS), ANL-HEP-PR-88-11, Nov. 1988; E. Elsen *et al.*(JADE), Z.Phys. **C46**, 349(1990); H. J. Behrend *et al.*(CELLO), DESY 89-125; W. Braunschweig *et al.*, DESY 90-047; H. Sagawa *et al.*(AMY), Phys. Rev. Lett. **63**, 2341(1989); J. Lim *et al.*(AMY), KEK 90-61, contribution to this conf.; I.Adachi *et al.*(TOPAZ), contribution to this conf.; K.Abe *et al.*(VENUS), contribution to this conf..
- [10] C. Albajar *et al.*(UA1), Phys. Lett. **B186**, 247(1987); H. R. Band *et al.*(MAC), Phys.Lett. **B200**, 221(1988); A. J. Weir *et al.*(Mark II), Phys. Lett. **B240**, 289(1990).
- [11] W. W. Ash *et al.*(MAC), Phys. Rev. Lett. **58**, 1080(1987); T. Greenshaw *et al.*(JADE), Z. Phys. **C41**, 1(1989); W. Braunschweig *et al.*(TASSO), DESY 88-100, July 1988; D. Stuart *et al.*(AMY), Phys. Rev. Lett. **64**, 983(1990); K. Abe *et al.*(VENUS), Phys. Lett. **B232**, 425(1989); I.Adachi *et al.*(TOPAZ), contribution to this conf.
- [12] W. Braunschweig *et al.*(TASSO), Z. Phys. **C41**, 385(1988); D. D. Pitzl *et al.*(JADE), Z. Phys. **C46**, 349(1990).
- [13] Y.C. Li *et al.*(AMY), Phys. Rev. **D41**, 2675(1990); H. Sagawa *et al.*(AMY), private communication for the NLL model analysis.
- [14] H. Aihara *et al.*(TPC/2 γ), Z. Phys. **C44**, 357(1989).
- [15] T. H. Burnett *et al.*(JACEE), Phys. Rev. Lett. **50**,2062(1983); G. J. Alner *et al.*(UA5), Phys. Rep. **154**, 247(1987); M. Adamus *et al.*(NA22), phys. Lett. **B185**, 200(1987); M. I. Adamovich *et al.*(EMU-01), Phys. Lett. **B201**, 397(1988).
- [16] A. Bialas and R. Peschanski, Nucl. Phys. **B273**, 703(1986).
- [17] W. Braunschweig *et al.*(TASSO), Phys. Lett. **B231**, 548(1989).
- [18] H. J. Behrend *et al.*(CELLO), contribution to this conf.
- [19] M. Feindt(CELLO), talk presented in this conf., to be published in Phys. Lett.**B**.
- [20] H. Aihara *et al.*(TPC/2 γ), UCLA-HEP-90-002, contribution to this conf.
- [21] W. Bartel *et al.*(JADE), Phys. Lett. **B104**, 325(1981); P. Baringer *et al.*(HRS), Phys. Rev. Lett. **56**, 1346(1986); C. de la Vaissiere *et al.*(MARKII), Phys. Rev. Lett. **54**, 2071 (1985); W. Braunschweig *et al.*(TASSO), Z. Phys. **C45**, 209(1989); H. Aihara *et al.*(TPC), Phys. Rev. Lett. **54**, 274(1985); P. Baringer *et al.*(HRS), Phys. Rev. Lett. **58**, 2627(1987); C. de la Vassiere *et al.*(MARKII), Phys. Rev. Lett. **58**, 644 (1987); C. de la Vassiere *et al.*(MARKII), Phys. Rev. Lett. **59**, 2412 (1987); H. Albrecht *et al.*(ARGUS),

- Phys. Lett. **B207**, 109(1988); T. Bowcock *et al.*(CLEO), Phys. Rev. Lett. **55**, 923(1985); C. de la Vassiere *et al.*(MARKII), Phys. Rev. Lett. **62**, 2444 (1989).
- [22] C. D. Buchanan and S. B. Chun, UCLA-HEP-90-003, contribution to this conf.
- [23] T. Kumita *et al.*(AMY), Phys. Rev. **D42** 1339(1990).
- [24] I. Adachi *et al.*(TOPAZ), Phys. Lett. **B234**, 525(1990).
- [25] I. Adachi *et al.*(TOPAZ), Phys. Lett. **B227**, 495 (1989).
- [26] K. Abe *et al.*(VENUS), KEK Preprint 90-4, to be published in Phys. Lett.**B**.
- [27] W. Braunschweig *et al.*(TASSO), Z. Phys. **C44**, 365(1989); W. Braunschweig *et al.*(TASSO), Z. Phys. **C42**, 17(1989).
- [28] I. H. Park *et al.*(AMY), Phys. Rev. Lett. **62**, 1713(1989); K. Abe *et al.*(VENUS), KEK 90-62, July 1990.
- [29] W. Braunschweig *et al.*(TASSO), Z. Phys. **C45**,1(1989).
- [30] Y. K. Kim *et al.*(AMY), Phys. Rev. Lett. **63**, 1772(1989); Y. K. Kim *et al.*(AMY), contribution to this conf.